Effect of main frequencies on characterizing fault damage zones using forward modeling and attribute of variance

Yangpu Chen[1], Zonghu Liao[2], Li-Yun Fu[3], Gang Zhou[4], Liang Xu[4], Kurt J. Marfurt[5], Xinru Mu[3], and Huayao Zou[2]

Abstract

Faulting processes have created large damage zones with complex structures in the field; however, estimating the width and geometry of such fault structures in the subsurface is challenging due to a lack of data. Seismic attributes (e.g., coherence and variance) from seismic surveys have been used for the characterization of faults, but most cases do not detail the effectiveness of this approach. By using forward modeling and the associated seismic attributes of variance, four fault models of idealized damage zones are characterized and the frequency effect is evaluated on the width estimation of fault damage zones in the subsurface. The main results indicate that (1) the general geometric pattern of damage zones could be identified by using simulated amplitude and seismic variance with main frequencies of 10, 25, and 40 Hz; (2) the estimated widths of damage zones at a low frequency of 10 Hz are larger (up to twofold) than those at frequencies of 25 and 40 Hz; for large damage zones (>400 m), the width is best estimated by a frequency of 25 Hz; and (3) scattering noise and diffraction around the fault are found in data at a high frequency of 40 Hz, which results in width overestimation of the damage zones by approximately 17%. The internal structures are difficult to distinguish as scattering noise and chaotic reflections dominate seismic signals. More factors that may influence the accuracy of damage zone width estimation via seismic attributes, include the bedding thickness, fracture density, and velocity. An in-depth understanding of this approach is useful in the application of seismic variance to characterize fault damage zones that may significantly control the fluid migration in the subsurface.

Introduction

Fault damage zones in the subsurface may display complex geometric shapes, with multiple interacted fault cores and surrounding damage zones, as observed in exposed structures (Figure 1; Aydin and Johnson, 1978; Faulkner et al., 2003; Liao et al., 2020). These damage zones form as a result of continued slip along the existing fault and ongoing fragmentation of the protolith. These damage zones usually occur at a later stage of fault evolution (Krantz, 1988; Cartwright et al., 1995). It is challenging to estimate the width of such complex damage zones in the subsurface due to lack of detailed data, which is critical to understand the internal structures and mechanical behavior, and to inform hydrological models (Caine et al., 1996; Faulkner et al., 2010; Busetti et al., 2012). The main objective here is to investigate the geometric features of damage zones using an approach of seismic simulation based on idealized fault models.

We recently developed four idealized fault models of damage zones (Liao et al., 2020) by using multiattribute analyses from a fine-resolution 3D seismic survey. The internal architecture and fracture distribution of the damage zones in the subsurface are set up for tight sandstone reservoirs in northeast Sichuan, China. The damage zones are mapped with widths in a range of 200–1000 m along faults ranging 3–15 km in length, and up to 1000 m of cumulative slip. We defined four idealized fault models based on the identification of numerous fault cores and associated damage zones,

[1]Chinese Academy of Sciences, Institute of Geochemistry, State Key Laboratory of Ore Deposit Geochemistry, Guiyang 550081, China and University of Chinese Academy of Sciences, Beijing 100049, China. E-mail: chenyangpu16@mails.ucas.ac.cn.

[2]China University of Petroleum (Beijing), State Key Laboratory of Petroleum Resources and Prospecting, Beijing 102249, China. E-mail: zonghuliao@163.com; zong@cup.edu.cn (corresponding author); huayaozou@cup.edu.cn.

[3]China University of Petroleum (East China), School of Geosciences, Qingdao, Shandong 266555, China. E-mail: lfu@upc.edu.cn; xinrumu@upc.edu.cn.

[4]PetroChina Southwest Oil and Gasfield Company, Chengdu 610000, China. E-mail: xu.liang@petrochina.com.cn, zhougang29@petrochina.com.cn.

[5]University of Oklahoma, School of Geosciences, Norman, Oklahoma 73019, USA. E-mail: kmarfurt@ou.edu.

Manuscript received by the Editor 22 January 2020; revised manuscript received 14 June 2020; published ahead of production 10 July 2020; published online 12 October 2020. This paper appears in *Interpretation*, Vol. 8, No. 4 (November 2020); p. SP157–SP165, 6 FIGS., 2 TABLES.

http://dx.doi.org/10.1190/INT-2020-0017.1.

including isolated, parallel, inosculation, and favored. Each of the models is attributed to proper faulting processes of the mechanical contrasts and fault-core distortion. Thus, we concluded that the derived models are realistic examples of complex damage zones in the subsurface (see the details in Liao et al., 2020).

The seismic attribute, variance, is defined as the coherent part of the seismic reflector divided by the average acoustic energy of the input seismic traces (Chopra and Marfurt, 2007). Trace-to-trace amplitude variation could be detected by variance attribute. Considering our interest is the feature of subsurface architecture, the seismic variance should be the appropriate attribute for this research.

In this study, we explore the effects of the seismic attribute, variance (the opposite of coherency), on the estimation of the damage-zone morphology in the subsurface, focusing on the effect of the main frequency on the width of damage zones. We applied forward simulations based on idealized fault models. Reverse time migration (RTM) is a useful tool for seismic imaging in complex structures, but it will produce low-frequency artifacts and distort seismic images with crosscorrelation imaging conditions (Rickett, 2003; Huang et al., 2015; Liu and Liu, 2018). Considering that reflectivity varies greatly in a damage zone, RTM was determined to not be an appropriate fit for simulation. Least-squares migration (LSM) is a linearized inversion method (Nemeth et al., 1999) and can give the true amplitude images that migration resolution is improved and migration artifacts are suppressed (Nemeth et al., 1999; Duquet et al., 2000; Fomel et al., 2002). However, LSM is a low-efficiency method. LSRTM, combining the LSM and RTM operators, can suppress low-frequency artifacts within RTM and has improved computation efficiency compared to LSM (Dai and Schuster, 2013; Huang et al., 2015; Liu and Liu, 2018). Thus, it is the chosen method for damage-zone simulation and provides reliable seismic attributes. We applied the least-squares reverse time migration (LSRTM) to simulation of the idealized damage-zone models.

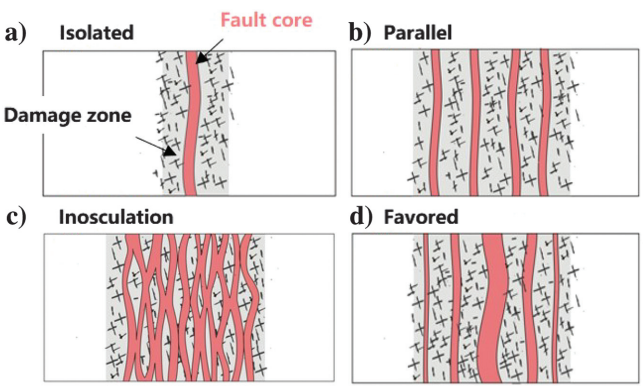

Figure 1. Schematic models of the damage zones adapted from Liao et al. (2020). (a) Isolated model: damage zone of the single fault core. (b) Parallel model: composite damage zone with approximately equal-size fault cores parallel/subparallel. (c) Inosculation model: composite damage zone with multiple, anastomosing fault cores. (d) Favored model: composite damage zone with one dominating fault core and a few secondary ones. The size is not to scale.

Seismic attributes are measures of seismic data that are used to visually enhance or quantify structures of interest in seismic images (Chopra and Marfurt, 2007). Seismic attributes, such as dip-azimuth (Marfurt and Kirlin, 2000; Guo et al., 2008; Liao et al., 2017), curvature (Roberts, 2001; Al-Dossary and Marfurt, 2006), coherence (Marfurt et al., 1998; Liao et al., 2019), and seismic variance (Marfurt and Rich, 2010; Liao et al., 2019), could efficiently be used to characterize appropriate fault zone architecture and properties. Seismic variance has demonstrated the ability to identify the general dimensions and shapes of damage zones, however, with limitations related to seismic noise and unknown complex features. It is evident that the seismic attribute contains noise that should be eliminated and does not always provide the best insight into the structures (Chopra and Marfurt, 2007; Li and Lu, 2014). How much noise contained within the seismic variance attribute becomes critical for determining the structure of the damage zones. With the expectation to quantify the effect from the seismic variance frequency on width estimation, for the idealized fault models of damage zones, we implement multiple forward simulations with various main frequencies and calculated attributes of variance correspondingly. The application of idealized fault models avoids background geologic noise. We propose that these simulations can be applied to the estimation of widths of the damage zones and also discuss the effect of main frequencies on the width error.

Model setup and approach

We analyze damage zones using forward modeling, and the approaches are shown below.

Geologic models of damage zones

Fault damage zones are commonly described to consist of a fault core and surrounding damage zone (Chester and Logan, 1986; Savage and Brodsky, 2011). Liao et al. (2020) propose four idealized fault models of damage zones (Figure 1) using a fine-resolution 3D seismic survey and associated seismic attributes, including

1) Isolated model for a typical damage zone of an independent fault, which is commonly discussed in outcrop research (Figure 1a).
2) Parallel model (Figure 1b) for a large composite damage zone with three large fault cores that are separated by corresponding damage zones. It is suggested that the parallel model is formed by the superposition of several subparallel faults of an approximately similar amount of slip that is spaced at equal distance from each other.
3) Inosculation model (Figure 1c) for a composite damage zone with multiple anastomosing fault cores and damage zones without individual fault cores.

It evolves by the coalescence of multiple, closely spaced fault segments that formed in earlier phases.

4) Favored model (Figure 1d) for a damage zone with multiple fault cores where the central fault core is the largest one that accommodates most of the deformation. It may start as a parallel model with multiple subparallel faults, and one fault core became weaker to accommodate additional deformation via localized slip in later stages. The central fault core is thus a favored slip surface.

Velocity models for damage zones

The damage zones likely consist of fragmented and fractured rock body with one or more fault cores of localized slip. The fragmented and fractured rock is known to influence the traveltimes and amplitudes of seismic waves (Anderson et al., 1974; Boadu and Long, 1996). Seismic waves will be attenuated when passing through the fractured medium, resulting in amplitude and amplitude-related seismic attributes attenuation (Maultzsch et al., 2007; Thompson et al., 2010). We applied a 2D seismic forward model, considering velocity models as analogs for realistic fault damage zones (Botter et al., 2014). We assumed that the protolith is homogeneous, and all faults are set with a dip angle of 81° and slip displacement of 50 m according to the field conditions. Considering that fractures are usually below the resolution of seismogram, the fractures in our models are represented as attenuated seismic velocities (Table 1):

$$\begin{cases} v_{pf} = v_{\text{pro}} \times 89\% \\ v_{sf} = v_{\text{pro}} \times 95\% \\ v_{\text{dam}} = v_{fc} + v' F(r) \end{cases}, \quad (1)$$

where $v_{pf}, v_{sf}, v_{\text{pro}}, v_{\text{dam}}$, and v_{fc} is the assumed velocities of primary fractures near the fault core, secondary fractures in the damage zones, protolith, damage zones, and fault core, respectively. The term v' is the velocity gradient between fault core and the protolith. The term $F(r)$ is a random function that describes the velocity increase gradually from fault core to the protolith (Maultzsch et al., 2007; Thompson et al., 2010; Faulkner et al., 2010). The geometric parameters are shown in Table 1 (Faulkner et al., 2010). Damage zones are idealized as approximately 1–2 orders wider than the fault cores (Sagy et al., 2001; Liao et al., 2019). The primary fractures are set near the fault core, and the secondary fractures are set in the damage zones with a random pattern. To study the impact of model setting, we designed four layers from 1000 to 2500 m for comparison (Figure 2), two thin beds in the shallow area and two thick beds in the deep area. Fracture density of the top bed and the bottom bed are set less than the middle two beds. These are idealized models to the problem, probably inaccurate, but it provides a reasonable approximation to model the damage zone in the sense of seismic attenuation (Anderson et al., 1974; Boadu and Long, 1996; Chopra and Marfurt, 2007; Li and Lu, 2014).

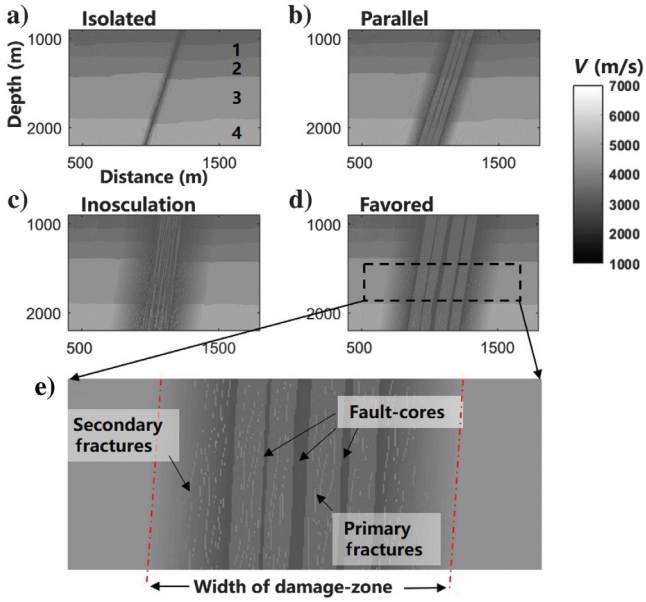

Figure 2. Idealized velocity models for forward modeling (a-d) correspond to the damage zones in Figure 1. (e). Schematic velocity setting for internal structure and fractures within the favored model of damage zone.

Table 1. Parameters of fault geometries.

Modeling parameters				Velocity parameters (m/s)		
Model size (m)		5000 × 3000		Protolith (v_{pro})	Primary fractures (v_{pf})	Secondary fractures (v_{sf})
Grid size (m)		5 × 5	Bed 1	3700	3293	3515
Sampling interval (ms)		5	Bed 2	3900	3471	3705
Source	Number	20	Bed 3	4400	3916	4180
	Interval (m)	250	Bed 4	4900	4361	4655
Fracture width (m)	Primary	2	Fault core (v_{fc})		3000λ	
	Secondary	1	Damage zone (v_d)		$v_{\text{dam}} = v_{fc} + v' F(r)$	

Seismic simulation and attribute of variance

We use the LSRTM theory to implement seismic imaging (Huang et al., 2015). The LSRTM simulator is based on wave equations using time extrapolation, which makes the simulation suitable for various structures with inclination angles and variation of transverse velocities.

The inputs for the LSRTM simulator include the velocity model, fracture setting (equation 1), grid size, observation system, and main frequency (Table 1). The velocity model is significant in determining the reflectivity with the contrast of velocities usually causing stronger seismic reflectivity. It is known that the wave velocity decreases approximately 50% within the fault core as estimated from in situ measurements or measurements on core samples in the laboratory (Nes et al., 2000). We assume that the velocity of fault core is 3000 m/s and beds with a velocity gradient as in Table 1. The velocity is set to increase from the fault core to the margin of the damage zone in the function of $F(r)$. The fault core is set independently from the beds to avoid the interaction of reflections. The spatial size of the models is set as 5000×3000 m, the grid size is 5×5 m, and the seismic sampling interval is 5 ms. A total of 20 sources are evenly distributed at 1 m depth with a spacing distance of 250 m. The other parameters are shown in Table 1.

To detect the discontinuities, faults, in the subsurface, we used the attribute of seismic variance, which integrates the cumulative seismic response to the structural deformation (Chopra and Marfurt, 2007; Iacopini and Butler, 2011; Liao et al., 2019). Variance can be described as the variation of amplitude:

$$V_{ij} = (A_{ij} - A_{\text{ave}})^2, \tag{2}$$

in which V_{ij} is the variance of ijth grid node, A_{ij} is the amplitude of ijth grid node, A_{ave} is the average amplitude. In a seismogram, the amplitude is a convolution of the wavelet and impedance. Wavelength, $\lambda = v/f$, is a function of frequency in our model. Variance, presented as equation 2, is obviously sensitive to the variation of amplitude from equation 1. The trace-to-trace variability is detected over a sample interval, and the large variance coefficients are used for delineation of the faults, whereas the low values are for the protolith. With fine resolution, it could be used for distinguishing the internal structure of the damage zones on a large scale. We thus expect the high-variance zone as the fault core and damage zones and low values for the protolith. This approach is usually applied using seismic reflection surveys, which has been validated to conform with field observations (Sagy et al., 2001; Mitchell and Faulkner, 2009; Savage and Brodsky, 2011). We adopt this approach for our forward modeling in this study.

Results

Fault damage zones

We applied LSRTM and the above approaches to obtain 12 simulations for four models of damage zones with main frequencies of 10, 25, and 40 Hz. The simulation results are illustrated via seismic amplitude with the zero-phase wavelet (Figure 3) and the seismic attribute of variance (Figure 4). Figure 3 displays seismic amplitude corresponding to vertical slices through the four models of damage zones with different main frequencies. We analyze the characteristics of damage zones based on the simulations.

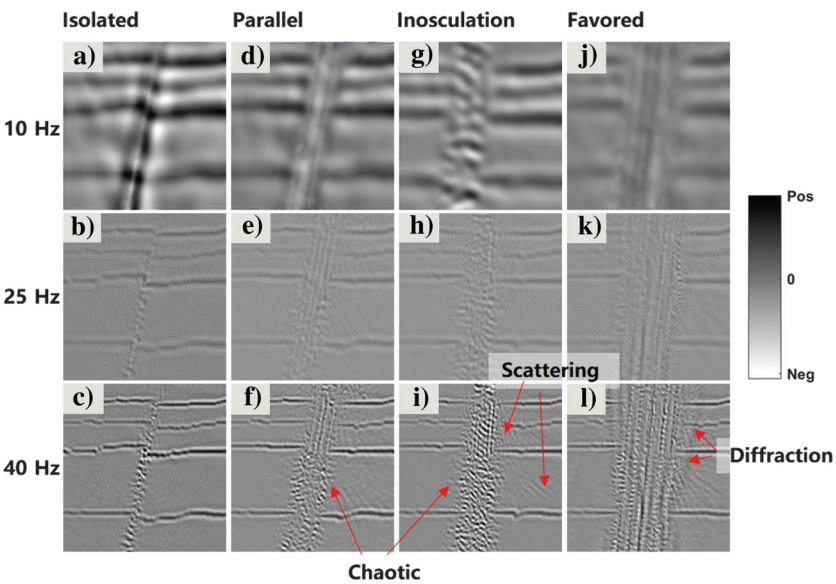

Figure 3. Fault detection by vertical slices through seismic amplitude. Results with main frequencies of 10, 25, and 40 Hz for the (a–c) isolated model, (d–f) parallel model, (g–i) inosculation model, and (j–l) favored model, respectively. Note the poor resolution in low frequencies (e.g., a, d, j, and g) and scattering, chaotic noises, and diffraction in (f, i, and l).

For the isolated model, the fault can be identified from the disturbance of amplitude waveforms for all three main frequencies (Figure 3a–3c). Figure 3a shows that dark and thick bands of waveforms appear horizontally for bed interfaces and vertically for the fault. These dark and thick bands turn much thinner at the main frequency of 40 Hz. It is difficult to identify the internal structure of damage zones of the isolated fault, particularly at 1800 m (the three beds, Figure 3a–3c), which could be attributed to the low resolution of the data and the relatively small size of the fault. The signal of waveform discontinuity for the fault is mixed with increasing noise from shallow to deep.

For the other three models, the general geometric shape of the damage zones could be recognized from the amplitude maps (Figures 3d–3l). The internal structures are unclear at the frequency of 10 Hz, but they could be delineated at higher frequencies of 25

and 40 Hz. Structural details, e.g., parallel fault cores, could be partially identified in Figure 3d–3e and the shallower area of Figure 3f. In a deep area of Figure 3f, noise occurred similar to what is observed for the isolated fault in Figure 3c. The structural details in Figure 3g–3l are not easily distinguished from the amplitude results for the rest of the models due to their structural complexities. Only the geometric patterns of large damage zones are shown, whereas the internal structures are not visible and are dominated by chaotic reflections in deep areas.

Widths of damage zones

We further investigate the seismic attribute of variance, which is a measurement of the discontinuity of a seismic section. Figure 4 presents the corresponding vertical profiles of seismic variance at the three main frequencies. The vertical zones of the red-yellow bands indicate the reverse faults. The high main frequencies of 25 and 40 Hz delineate the main damage zones of all of the damage-zone models. Compared to sections of amplitude, the noise in the deep area is filtered in seismic variance. The discontinuities in the red-yellow color vertically illustrate geometries of the damage zones. It is still difficult to elucidate the internal differences between the three models by seismic variance. Moreover, the low frequency of 10 Hz produces significant noise around the damage zones, for example, large bright patches near the faults that would lead to misinterpretation as discontinuities (Figure 4a). Figure 4d shows smaller damage zones in shallow areas for the parallel model and, in contrast, exaggerated damage zones in the deep area. Figure 4g illustrates the bifurcation of faults in shallow areas for the inosculation model, which is not the case in our geology model. These are examples caused by poor resolutions due to low frequencies.

To further explore the effect of frequency on characterizing the damage zones, we followed the approach of Liao et al. (2019) to apply seismic variance to estimate the widths of the damage zones. We prepared 84 profiles of seismic variance (Figures 5and 6) crossing the faults in 1500–1800 m. The seven profiles in each section display distribution of the seismic variance for one main frequency, which we generalized as the characteristics of one of the damage zones. A typical damage zone, e.g., an isolated model, could be represented by a zone of high variance, 0.1–0.9 (gray in Figure 5a–5c). We argue that a small fraction of the highest variance, >0.8, could be interpreted as the fault core (Liao et al., 2019). The width of the damage zone is estimated to be 400 m using main frequencies of 10 Hz, and it decreases to 250 and 200 m at the main frequencies of 25 and 40 Hz, respectively. The distribution of seismic variance in the frequency of 10 Hz (Figure 5a) obviously does not comply with the damage zones in Figure 5b–5c in two aspects: (1) the widths are different, and (2) the structure is distorted at low frequency.

For the other three models, we also prepared the profiles of distributions of seismic variance. The widths are estimated, and structures are evaluated based on the profiles from the 10, 25, and 40 Hz main frequencies, respectively. As shown for the parallel model in Figure 5d–5l, the widths of the damage zones are varied with few differences for two reasons: (1) the profiles are selected from the deep area that avoids the aforementioned exaggeration (the isolated model) in the shallow area and (2) these damage zones are set with a relatively large scale (>400 m) compared to the isolated fault, which is now distinguishable at a low frequency. Another essential feature is the profiles of the seismic variance show small values (approximately 0) for the protolith, which is due to the idealized background setting that is not realistic in nature. Similar observations are found for the inosculation and favored models.

Discussions

LSRTM was used to simulate the characterizations of four idealized fault model of damage zones. If we could build a damage-zone velocity model with the main features fitting to nature, and the simulation setting (e.g., grid size) is suitable, the simulation would provide us a feasible way to evaluate the effect of frequency on the estimation of damage-zone width.

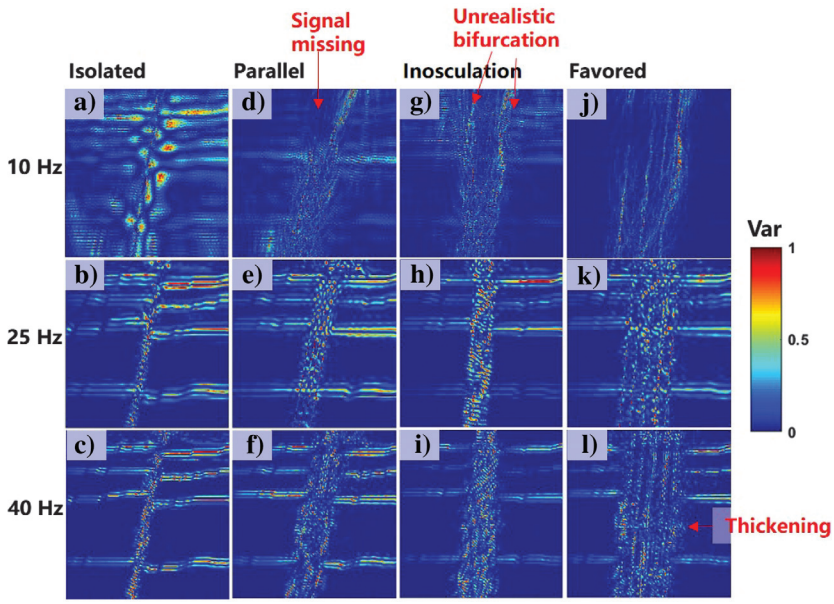

Figure 4. Fault detection by vertical slices through seismic attributes of variance. Results of attribute variance with main frequencies of 10, 25, and 40 Hz for the (a–c) isolated model, (d–f) parallel model, (g–i) inosculation model, and (j–l) favored model, respectively. Note the (a) scattering patches, (g) unrealistic fault bifurcation, and (l) thickening.

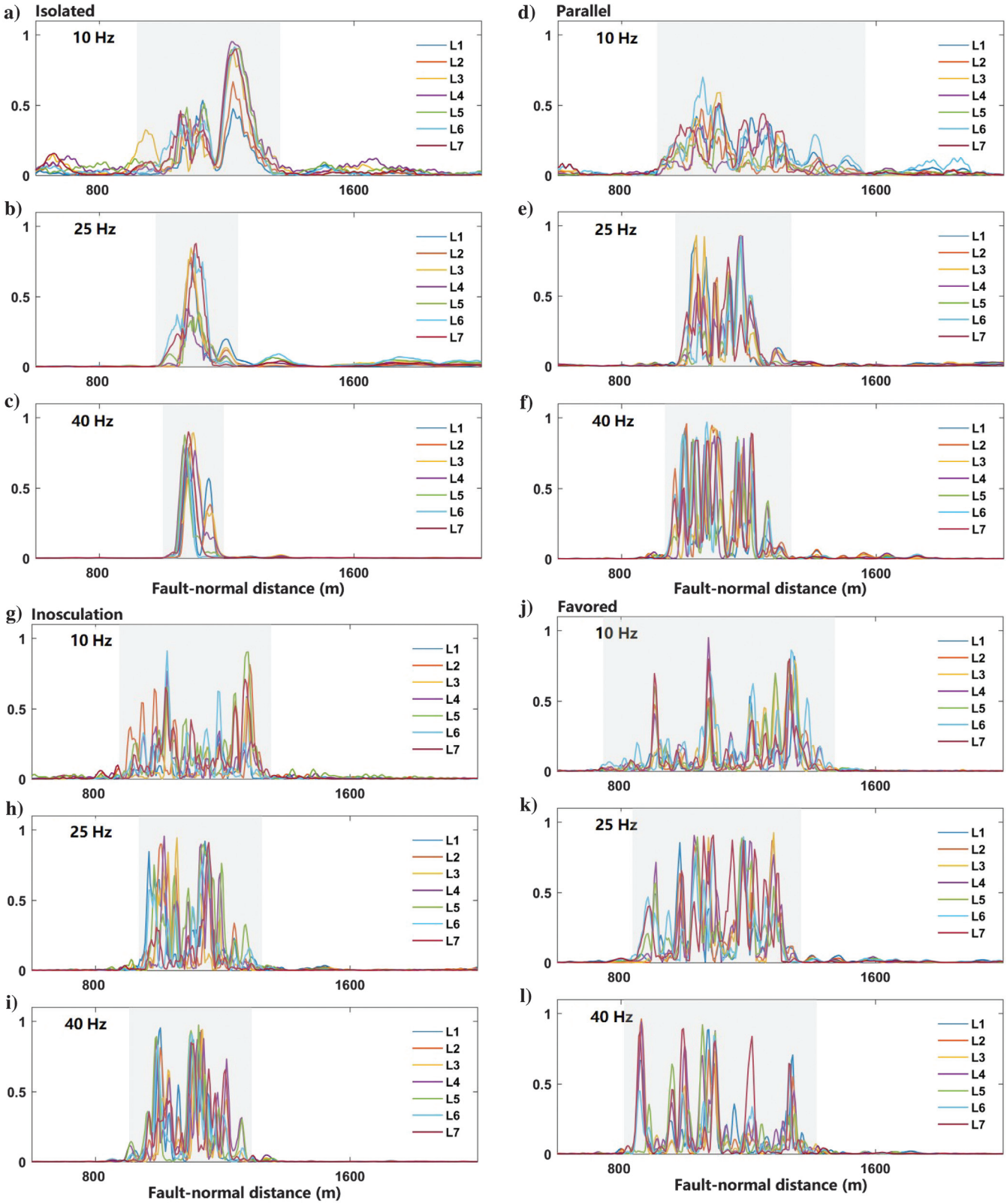

Figure 5. Profiles of the seismic variance values across the damage zones. Profiles of attribute variance with main frequencies of 10, 25, and 40 Hz for (a–c) isolated model, (d–f) parallel model, (g–i) inosculation model, and (j–l) favored model, respectively. Profiles locations in Figure 2e; variance values above the background are interpreted as damage zones (the gray zone).

Bed thickness, fracture density, and velocity gradient

We first discuss how the velocity models affect the quality of our simulation results. In the case of a frequency of 40 Hz, the relationship between fracture density and imaging quality is clearly presented (Figures 3 and 4). In the third bed that is set thick (500 m) with high fracture density, the reflection of the damage zones is detected with more noise due to chaotic reflections than in the fourth bed with less fracture density. The chaotic noise widens the width of damage zones and decreases the visibility of the structure details (e.g., Figure 3f). For the second bed that is set thin (200 m) with a high fracture intensity in the shallow area, the structure details are better preserved by the seismic signal and are illustrated, e.g., in Figure 3c, 3f, and 3i. Compared to the third bed that is thick, it illustrates that there is less chaotic reflection but more seismic scattering in the shallow areas with lower seismic velocity. The results show that the bed-controlled fracture density and velocity gradient could cause different types of noise, significantly affecting the interpretation results using amplitude and seismic variance.

Spectral effect on the estimation of widths

LSRTM is a relatively accurate migration method based on data simulated by the finite difference method (Huang et al., 2015). Besides the grid size limited by computing power, frequency is the main factor to affect simulated results (Figures 3 and 4). We set the main frequencies as 10, 25, and 40 Hz to analyze how the fault damage zones can be imaged. In general, the higher the wave frequency is, the smaller the size of geologic bodies can be resolved by seismic wavelet. Figure 6 shows the main frequencies in relation to the widths of damage zones (Table 2). The red lines are for the actual width of damage zones by the model setting; the blue lines are widths estimated from the simulation results. For the isolated model with a damage zone of 180 m in width, the higher the frequency, the more accurate the estimation; for the parallel model and inosculation model with large damage zones (>400 m), there is not much difference between frequencies of 25 and 40 Hz. As for the favored model, only a frequency of 25 Hz best fits the actual width; both of the results from the low frequency of 10 Hz and a high value of 40 Hz suffer from the influence of noise. With regard to the high frequency in the example of 40 Hz for the favored model, diffraction around the fault is found. Mixed with scattering noise, it will lead to width overestimation of the damage zones, e.g., approximately 17% for the favored model. The Fresnel zone (Kozlov, 2014) could result in the overestimation of the width of damage zone in a low frequency (e.g., the isolated model of 10 Hz) in small fault damage zones, whereas the overestimation by the Fresnel zone could hardly be seen in large fault damage zones (e.g., composite damage zones).

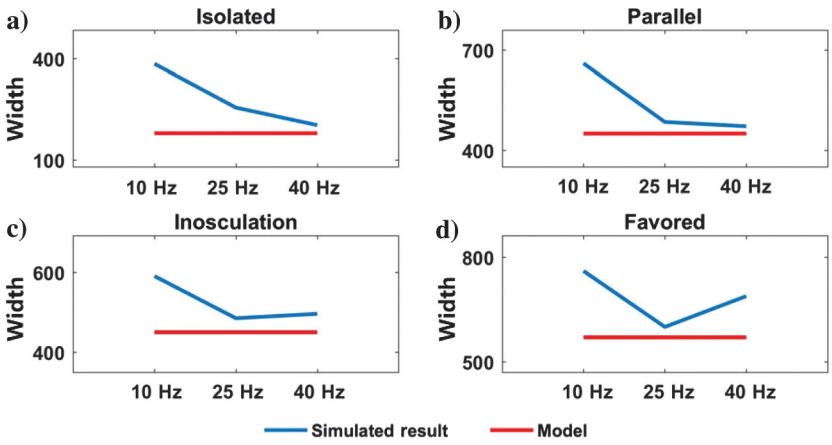

Figure 6. Width estimation from the seismic variances (Figure 6) versus frequencies for the (a) isolated model, (b) parallel model, (c) inosculation model, and (d) favored model. The red line illustrates the actual widths from the models.

Our results illustrate that the structural details of the three composite models of damage zones are challenging to detect, which is possibly limited by the resolution of the seismic data. The accumulated, distorted signal also could be attributed to the noise of chaotic reflection in the deep subsurface. However, it is feasible to apply the seismic attribute of variance to measure the widths of damage zones (>200 m) with acceptable overestimations. We failed to qualitatively define all the styles of fault damage zones because of the scattering noise from the fault zones. It strongly depends on the size of the structures that deserves investigation in the future. For wide damage zones (>400 m), the

Table 2. Damage zones width and resolution (λ).

	Model	10 Hz		25 Hz		40 Hz	
	Width (m)	Width (m)	λ (m)	Width (m)	λ (m)	Width (m)	λ (m)
Isolated	180	385	300–490	256	120–196	204	75–123
Parallel	450	660		485		472	
Inosculation	465	590		485		496	
Favored	570	760		600		668	

distribution of damage zones and internal structures can be interpreted by seismic attributes integrated with geologic modeling and outcrop observations.

Summary

In this study, we displayed an approach to apply seismic simulation to characterize the structure of damage zones and evaluate the frequency effect on the estimation of damage-zone widths. Though the internal structures of the damage zones are hard to distinguish, the widths of the damage zones could be calculated with some overestimation using seismic attributes at different main frequencies of 10, 25, and 40 Hz. Such overestimation, which appeared in previous attribute analyses of seismic surveys, could be complemented by using higher frequency, e.g., 25 and 40 Hz, to improve the signal-to-noise ratio. It is, therefore, shown that seismic variance can be applied to characterize the widths of fault damage zones, which will further provide insights for evaluating the internal structures of faults.

Acknowledgments

The authors would like to thank the reviewers, B. Carpenter, and the Attribute Assisted Seismic Processing and Interpretation (AASPI), University of Oklahoma. Support funds were provided by National Key Research and Development Program of China (No. 2019YFC0605502) and Strategic Priority Research Program of the Chinese Academy of Sciences (Nos. XDA14010306 and XDA14010303).

Data and materials availability

Data associated with this research are available and can be obtained by contacting the corresponding author.

References

Al-Dossary, S., and K. J. Marfurt, 2006, 3D volumetric multispectral estimates of reflector curvature and rotation: Geophysics, **71**, no. 5, P41–P51, doi: 10.1190/1.2242449.

Anderson, D. L., B. Minster, and D. Cole, 1974, Effect of oriented cracks on seismic velocities: Journal of Geophysical Research, **79**, 4–4015, doi: 10.1029/JB079i026p04011.

Aydin, A., and A. M. Johnson, 1978, Development of faults as zones of deformation bands and as slip surfaces in sandstone: Pure and Applied Geophysics, **116**, 931–942, doi: 10.1007/BF00876547.

Boadu, F. K., and L. T. Long, 1996, Effects of fractures on seismic-wave velocity and attenuation: Geophysical Journal International, **127**, 86–110, doi: 10.1111/j.1365-246X.1996.tb01537.x.

Botter, C., N. Cardozo, S. Hardy, I. Lecomte, and A. Escalona, 2014, From mechanical modeling to seismic imaging of faults: A synthetic workflow to study the impact of faults on seismic: Marine and Petroleum Geology, **57**, 187–207, doi: 10.1016/j.marpetgeo.2014.05.013.

Botter, C., N. Cardozo, S. Hardy, I. Lecomte, G. Paton, and A. Escalona, 2016, Seismic characterization of fault damage in 3D using mechanical and seismic modeling: Marine and Petroleum Geology, **77**, 973–990, doi: 10.1016/j.marpetgeo.2016.08.002.

Busetti, S., K. Mish, P. Hennings, and Z. Reches, 2012, Damage and plastic deformation of reservoir rocks — Part 2: Propagation of a hydraulic fracture: AAPG Bulletin, **96**, 1711–1732, doi: 10.1306/02011211011.

Caine, J. S., J. P. Evans, and C. B. Forster, 1996, Fault zone architecture and permeability structure: Geology, **24**, 1025–1028, doi: 10.1130/0091-7613(1996)024<1025:FZAAPS>2.3.CO;2.

Cartwright, J. A., B. D. Trudgill, and C. S. Mansfield, 1995, Fault growth by segment linkage: An explanation for scatter in maximum displacement and trace length data from the Canyonlands Grabens of SE Utah: Journal of Structural Geology, **17**, 1319–1326, doi: 10.1016/0191-8141(95)00033-A.

Chester, F. M., and J. M. Logan, 1986, Implications for mechanical properties of brittle faults from observations of the Punchbowl Fault Zone, California: Pure and Applied Geophysics, **124**, 79–106, doi: 10.1007/BF00875720.

Chopra, S., and K. J. Marfurt, 2007, Seismic attributes for prospect identification and reservoir characterization: SEG.

Dai, W., and G. T. Schuster, 2013, Plane-wave least-squares reverse-time migration: Geophysics, **78**, no. 4, S165–S177, doi: 10.1190/geo2012-0377.1.

Duquet, B., K. J. Marfurt, and J. Dellinger, 2000, Kirchhoff modeling, inversion for reflectivity, and subsurface illumination: Geophysics, **65**, 1195–1209, doi: 10.1190/1.1444812.

Faulkner, D. R., C. A. L. Jackson, R. J. Lunn, R. W. Schlische, Z. K. Shipton, C. A. J. Wibberley, and M. O. Withjack, 2010, A review of recent developments concerning the structure, mechanics and fluid flow properties of fault zones: Journal of Structural Geology, **32**, 1557–1575, doi: 10.1016/j.jsg.2010.06.009.

Faulkner, D. R., A. C. Lewis, and E. H. Rutter, 2003, On the internal structure and mechanics of large strike-slip fault zones: Field observations of the Carboneras fault in southeasten Spain: Tectonophysics, **367**, 235–251, doi: 10.1016/S0040-1951(03)00134-3.

Fomel, S., J. Berryman, R. Clapp, and M. Prucha, 2002, Iterative resolution estimation in least-squares Kirchhoff migration: Geophysical Prospecting, **50**, 577–588, doi: 10.1046/j.1365-2478.2002.00341.x.

Guo, H., S. Lewis, and K. J. Marfurt, 2008, Mapping multiple attributes to three- and four-component color models — A tutorial: Geophysics, **73**, no. 3, W7–W19, doi: 10.1190/1.2903819.

Huang, J., C. Li, R. Wang, and Q. Li, 2015, Plane-wave least-time reverse time migration for rugged topography: Journal of Earth Science, **26**, 471–480, doi: 10.1007/s12583-015-0556-5.

Iacopini, D., and R. W. H. Butler, 2011, Imaging deformation in submarine thrust belts using seismic attributes: Earth and Planetary Science Letters, **302**, 414–422, doi: 10.1016/j.epsl.2010.12.041.

Kozlov, E. A., 2014, Pressure-dependent seismic response of fractured rock: Geophysics, **69**, 877–1103, doi: 10.1190/1.1778232.

Krantz, R. W., 1988, Multiple fault sets and three dimensional strain: Theory and application: Journal of Structural Geology, **10**, 225–237, doi: 10.1016/0191-8141(88)90056-9.

Li, F., and W. Lu, 2014, Coherence attribute at different spectral scales: Interpretation, **2**, no. 1, SA99–SA106, doi: 10.1190/INT-2013-0089.1.

Liao, Z., W. Li, H. Zou, F. Hao, K. J. Marfurt, and Z. Reches, 2020, Composite damage zone in the subsurface: Geophysical Journal International, **222**, 225–230, doi: 10.1093/gji/ggaa158.

Liao, Z., H. Liu, B. M. Carpenter, K. J. Marfurt, and Z. Reches, 2019, Analysis of fault damage-zones by using 3D seismic coherence in Anadarko Basin, Oklahoma: AAPG Bulletin, **103**, 1771–1785, doi: 10.1306/1219181413417207.

Liao, Z., H. Liu, Z. Jiang, K. J. Marfurt, and Z. Reches, 2017, Fault damage zone at subsurface: A case study using 3D seismic attributes and a clay model analogue for the Anadarko Basin, Oklahoma: Interpretation, **5**, no. 2, T143–T150, doi: 10.1190/INT-2016-0033.1.

Liu, X., and Y. Liu, 2018, Plane-wave domain least-squares reverse time migration with free-surface multiples: Geophysics, **83**, no. 6, S477–S487, doi: 10.1190/geo2017-0570.1.

Marfurt, K. J., and R. L. Kirlin, 2000, 3-D broad-band estimates of reflector dip and amplitude: Geophysics, **65**, 304–320, doi: 10.1190/1.1444721.

Marfurt, K. J., R. L. Kirlin, S. L. Farmer, and M. S. Bahorich, 1998, 3-D seismic attributes using a semblance-based coherency algorithm: Geophysics, **63**, 1150–1165, doi: 10.1190/1.1444415.

Marfurt, K. J., and J. Rich, 2010, Beyond curvature — Volumetric estimates of reflector rotation and convergence: 80th Annual International Meeting, SEG, Expanded Abstracts, 1467–1472, doi: 10.1190/1.3513118.

Maultzsch, S., M. Chapman, E. Liu, and X. Li, 2007, Modelling and analysis of attenuation anisotropy in multi-azimuth VSP data: Geophysical Prospecting, **55**, 627–642, doi: 10.1111/j.1365-2478.2007.00645.x.

Mitchell, T. M., and D. R. Faulkner, 2009, The nature and origin of off fault damage surrounding strike-slip fault zones with a wide range of displacements: A field study from the Atacama fault system, northern Chile: Journal of Structural Geology, **31**, 802–816, doi: 10.1016/j.jsg.2009.05.002.

Nemeth, T., C. Wu, and G. Schuster, 1999, Least-squares migration of incomplete reflection data: Geophysics, **64**, 208–221, doi: 10.1190/1.1444517.

Nes, O. M., R. M. Holt, and E. Fjær, 2000, The reliability of core data as input to seismic reservoir monitoring studies: Society of Petroleum Engineers, **5**, 79–86, doi: 10.2118/65180-MS.

Rickett, J., 2003, Illumination-based normalization for wave-equation depth migration: Geophysics, **68**, 1371–1379, doi: 10.1190/1.1598130.

Roberts, A., 2001, Curvature attributes and their application to 3D interpreted horizons: First Break, **19**, 85–100, doi: 10.1046/j.0263-5046.2001.00142.x.

Sagy, A., Z. Reches, and I. Roman, 2001, Dynamic fracturing: Field and experimental observations: Journal of Structural Geology, **23**, 1223–1239, doi: 10.1016/S0191-8141(00)00190-5.

Savage, H. M., and E. E. Brodsky, 2011, Collateral damage: Evolution with displacement of fracture distribution and secondary fault strands in fault damage-zones: Journal of Geophysical Research, **116**, 428–452, doi: 10.1029/2010JB007665.

Thompson, M. D., A. M. Grunow, and J. Ramezani, 2010, Cambro-Ordovician paleogeography of the Southeastern New England Avalon Zone: Implications for Gondwana breakup: Geological Society of America Bulletin, **122**, 76–88, doi: 10.1130/B26581.1.

Biographies and photographs of the authors are not available.